Performance Impact of Fast Flow Paths Through Grout Monoliths Used for Radioactive Waste Disposal – 13224

Cynthia L. Dinwiddie*, Gary R. Walter*, David W. Esh** and Cynthia S. Barr**
*Southwest Research Institute (SwRI®), Geosciences & Engineering Division, San Antonio, Texas
cdinwiddie@swri.org
**U.S. NRC, Office of Federal and State Materials and Environmental Management Programs, Division of Waste Management and Environmental Protection, Rockville, Maryland

ABSTRACT

Empty HLW handling and storage tanks at SRS and INL contain residual radioactivity; these tanks are being stabilized with cementitious grout during closure operations. The US NRC directed the Center for Nuclear Waste Regulatory Analyses (CNWRA®) to develop physical analogs of cementitious grout monoliths to investigate their potential to form fast flow pathways such as macrocracks, separations between grout lifts, and annuli around pipes, supports, and along tank walls. CNWRA developed and tested 15 55-gal-drum–scale specimens and 2 larger specimens of tank-filling cementitious grout, and 9 specimens of pipe-filling grout. These experiments demonstrated that the size of fast flow pathways that develop and the peak temperatures attained during hydration are proportional to the scale of the specimen, and that annular apertures and bulk grout permeability generally increased with time post-placement. Cracks developed overnight following placement of each grout lift in the largest specimen, but developed more slowly in smaller specimens, perhaps due to a ~20 °C difference in peak temperatures, which influence the thermal gradients that can induce cracking. Plastic and drying shrinkage commonly led to poor grout-to-metal and grout-to-grout bonding. Cracks, annular gaps, and grout flow lobe seams transmitted fluids during injection testing. Macroscale flow pathways such as these are not readily observed in bench-scale specimens of cementitious tank grout.

INTRODUCTION

US DOE is in the process of closing HLW tanks at SRS and INL under the Ronald W. Reagan National Defense Authorization Act of 2005 (NDAA). DOE may physically and chemically stabilize NDAA waste tanks with cementitious grout to limit waste release through hydraulic and chemical control. DOE may rely on engineered barrier properties that provide attenuation and retardation of radionuclide migration to demonstrate compliance with performance objectives.

NRC reviews of DOE waste determinations and performance assessments for HLW tank closure have indicated that fast flow paths through cementitious grout may dominate waste release [1]. Fast pathways may consist of macrocracks, separations between grout lifts, and annular gaps around pipes, supports, and along tank walls. Because of the unique structure and large size of HLW tanks {e.g., diameters range from 3.5 to 26 m and heights/lengths range from 6.4 to 11.6 m [2, 3]} and the novel grout formulations being used, few empirical data were available from which to estimate the likelihood of formation and properties of fast pathways that might develop in them. To understand the potential for fast flow path formation through or around stabilizing grout, CNWRA developed grout monoliths to investigate these features and gain insight into risk-significant aspects of grout behavior and properties that affect performance.

METHODS

Grout monoliths of three scales were developed to investigate the potential for fast flow paths to form within the first several years after grout placement. Grout specimens were instrumented to permit observation and quantification of (i) temperatures attained during hydration, (ii) macrocrack and vug characteristics, (iii) shrinkage annuli and (iv) separations between distinct units of grout. Analyses included pneumatic testing of grout permeability and annular apertures that surround embedded pipes to evaluate temporal evolution; borescopic observations of grout structures; crack characterization; dye-tracer slug testing to identify interconnected fast pathways and seeps, and pressure responses to slug pulsing. Monoliths ranged from the 55-gal-drum size (i.e., nominal diameter and height of 61 and 88 cm) to a cylindrical specimen with 3-m radius and 0.8-m thickness.

Fifteen drum-scale grout specimens (Fig. 1A) were developed and tested. Copper tubing, black steel pipes, and thermocouples were suspended in carbon steel drums prior to grout placement to simulate cooling coils and other internal fixtures and to measure temperatures. The black steel pipe was also used for gas injection testing. Glass tubes were suspended within so that vugs and grout lift interfaces could be observed via borescope. All drums were insulated at their circumference and base with R-13 fiberglass and then re-wrapped at their circumference with a foil-faced bubble wrap radiant barrier [4].

Drum specimens are composed of six grout types: SRS-like strong grout [5], SRS-like reducing grout, SRS-like next-generation, sand-based and gravel-based reducing grouts, INL-like controlled low-strength material (CLSM) [6], and INL-like heel grout [7]. Batch details were reported in [4, 8].

Next, a sector-shaped specimen (Fig. 1B) was developed to investigate the size of annular gaps that develop surrounding pipes in larger monoliths; it was insulated with R-13 fiberglass along both radial boundaries to simulate lateral heat flow conditions within an NDAA tank, but was not insulated at the external arc boundary. This specimen was constructed over the course of 3 days by filling the form with one lift of SRS-like reducing grout followed by two lifts of an SRS-like strong grout. Grout was transferred from the mixer to the form by wheelbarrow. Batch details were reported in [4]. Thermocouples suspended within the form recorded temperature evolution.

To determine the size of internal gaps that develop between pipes and internal pipe grout [9], a pipe grout batch was prepared to seal 9 black steel pipes (5-cm diameter) embedded in some of the aforementioned tank grout specimens (Fig. 1) {details were reported in Appendix A of [4]}.

Finally, a cylindrical grout specimen (Fig. 1C) was placed within an uninsulated, outdoor tank on a level gravel pad; this specimen was subject to differential diurnal solar heating and cooling. It was constructed with a SRS-like next-generation sand-based reducing grout that was consistent with a formulation reported by [5, 6], and was placed in three lifts on 3 consecutive days [8]. The tank was instrumented with thermocouples to record temperatures during grout hydration; three black steel pipes were suspended within the tank to investigate the size of annular gaps that developed around them. To minimize evaporative water loss and maintain humid conditions, the tank was covered with heat-shrink plastic after grouting operations each day; the sheeting was heat shrunk to the tank after the last batch was placed where it remained for 1 month.

Fig. 1. (A) 55-gal drum-scale tank grout specimens. (B) Sector-shaped specimen, having 3-m radius by 30° arc by 0.8-m thickness. Pipes suspended in (A) and (B) were later filled with pipe grout. (C) Cylindrical specimen, 12× larger than sector, placed in a 0.63-cm-thick-walled tank, 6.1-m-diameter by 0.9-m-deep. (D) Cracked core extracted for analysis from (C).

Each grout specimen was evaluated for shrinkage by injecting gas into the embedded pipes at a specified pressure and measuring the flow rate [4, 8, 10] to assess the size of annular gaps that formed around them. Grouted pipes were tested similarly to determine whether internal annuli had developed between the pipe grout and the pipe. After each set of pressure and flow rate data pairs had been acquired, the surfaces of grout specimens were doused with a thin film of water to enable visual identification of bubbles indicating the location of fast flow pathways and their relative intensities.

Annular gap calculations used the analytical solution for incompressible fluid flow through a continuous annulus described by [11] (their p. 53, Eq. 2.4-16), assuming flow through the grout mass is negligible. Internal pipe grout apertures were calculated using the same solution, assuming the flow path was the sum of the length of pipe grout inside the pipe plus the length of tank grout outside the pipe. The calculated value represents a composite approximation of apertures inside and outside the pipe because it does not account for the flow reversal that occurred at the distal end of the pipe (which involves a pressure loss that underestimates the gap aperture) or for compressible gas flow.

Another form of shrinkage assessment utilized the zero-degree longitudinal ultrasonic pulse-echo inspection technique [12] on a 5-cm × 5-cm grid to survey 36% of the steel tank liner surrounding the relatively large cylindrical grout specimen for air gaps at the interface between the grout and the tank liner.

Pressure and flowrate data from gas injection tests of embedded pipes were inverted to also estimate effective bulk grout permeability [10]. An injection pressure–steady gas flow rate correlation developed with the numerical gas flow code BioGas Emissions Model (BIGEM) [13] was used, which assumes Darcian and ideal gas compressible fluid flow throughout the grout matrix under moderate pressure.

The apparent annulus aperture and effective gas permeability solutions represent two bounding conceptual models for gas flow through the monoliths, which were solved to estimate upper bounding parameters. Gas flow through the pipe annulus was not measured separately from advective flow through the grout, so the pneumatic data represent an uncertain combination of advective and annular flow.

Gas injection tests were also performed of packed-off intervals of coreholes that had been drilled into the cylindrical grout specimen. Gas was injected through a mechanical pipe packer while measuring the flow rate at constant pressure. BIGEM corehole models [8] utilized a 2D axisymmetric finite-difference grid to account for grout thickness at the corehole location, corehole depth, and packer position.

Gas injection testing does not identify preferential flow pathways between coreholes and the monolith perimeter. Therefore, three-color fluorescent-dye–tracer slug tests also were performed of the relatively large cylindrical specimen to obtain information about the permeability of its macrocracks and the locations and connectivity of its preferential flow paths. Slug testing introduced controlled volumes of dye tracer into individual coreholes while simultaneously monitoring pressure in all nine coreholes. Coreholes were sequentially tested as dye-tracer sources to link them to breakthroughs at other coreholes or at the monolith perimeter. Removal of the steel liner from the specimen facilitated direct observation of the tracers as they broke through the perimeter. A rough estimate of the order of magnitude of grout permeability was estimated via the relationship given by [14] (their Eqs 5-38 to 5-40).

Cracks exposed on the surface of the second and third lifts of the cylindrical grout monolith were characterized by mapping their locations and variable apertures. Crack characteristics of the third lift were correlated with topographic data obtained from a laser scanning survey. Cracks were also characterized where they intersected three cores (Fig. 1D), nine coreholes, and specimen sidewalls.

RESULTS AND DISCUSSION

Grout Flow During Placement

Grout lift surfaces were categorized as smooth (e.g., SRS-like strong grout; SRS-like next-generation, gravel-based reducing grout); billowy/ropy (e.g., SRS-like reducing grout; SRS-like next-generation, sand-based reducing grout); lumpy (i.e., INL-like heel grout) or smooth-to-rough (i.e., INL-like CLSM) (Fig. 2A–D). A relatively smooth grout surface is consistent with a very flowable, relatively self-leveling cementitious material. Ropy, rippled grout surfaces are consistent with relatively flowable, but non-self-leveling cementitious material. Borescopic and sidewall observations both indicate that fresh grout placed onto the variable topography of an underlying lift does not completely fill available void space (e.g., Fig. 2E) [4]. CLSM characterized as smooth-to-rough exhibited solid–liquid segregation during placement: solids submerged below a liquid layer cured in a very smooth, platy fashion, but solids left standing above the liquid layer cured with rough patches. The non-self-leveling behavior of INL-like heel grout is consistent with its intended purpose, which is to corral residual liquids for final pumped removal {Appendix C-1 of [1]}; however, hydrated heel grout is also highly permeable.

As grout flows around obstacles, the grout mass separates on the leading edge and two grout flow lobes connect on the trailing edge (Fig. 2F) forming a topographically indented seam. As grout continues to be placed, the seam may grow to become a vertically oriented planar structure; shrinkage at the seam results in it behaving as a preferential flow path [10]. Likewise, horizontal seams may form at lift and lobe interfaces as a result of shrinkage that occurs at the boundary between two grout masses placed at different times.

Grout batches prepared for the large cylindrical specimen met slump flow specifications, but the grout was non-self-leveling (Fig. 1C). As a result, each lift varied spatially in volume, thickness, and topography; subsequent lifts did not completely cover previous lifts (Fig. 2G).

Grout Temperatures and Temperature Gradients

Fully insulated, SRS-like next-generation, sand-based reducing grout drum-scale specimens attained peak temperatures that were ~20 °C cooler than occurred within the larger, uninsulated, cylindrical grout specimen. Heating rate and peak temperature attained were positively correlated to the fraction of Portland cement relative to other pozzolanic materials (blast furnace slag cement and fly ash) and inert materials (sand and pea gravel) in the grout formulations. Temperature data and visual observations indicated that formulations having relatively little Portland cement and relatively more fly ash, blast furnace slag cement, or inert pea gravel cured relatively slowly and remained gelatinous for more than 24 hrs. This behavior is consistent with slow rates of hydration for fly ash and blast-furnace slag cement reported by [15].

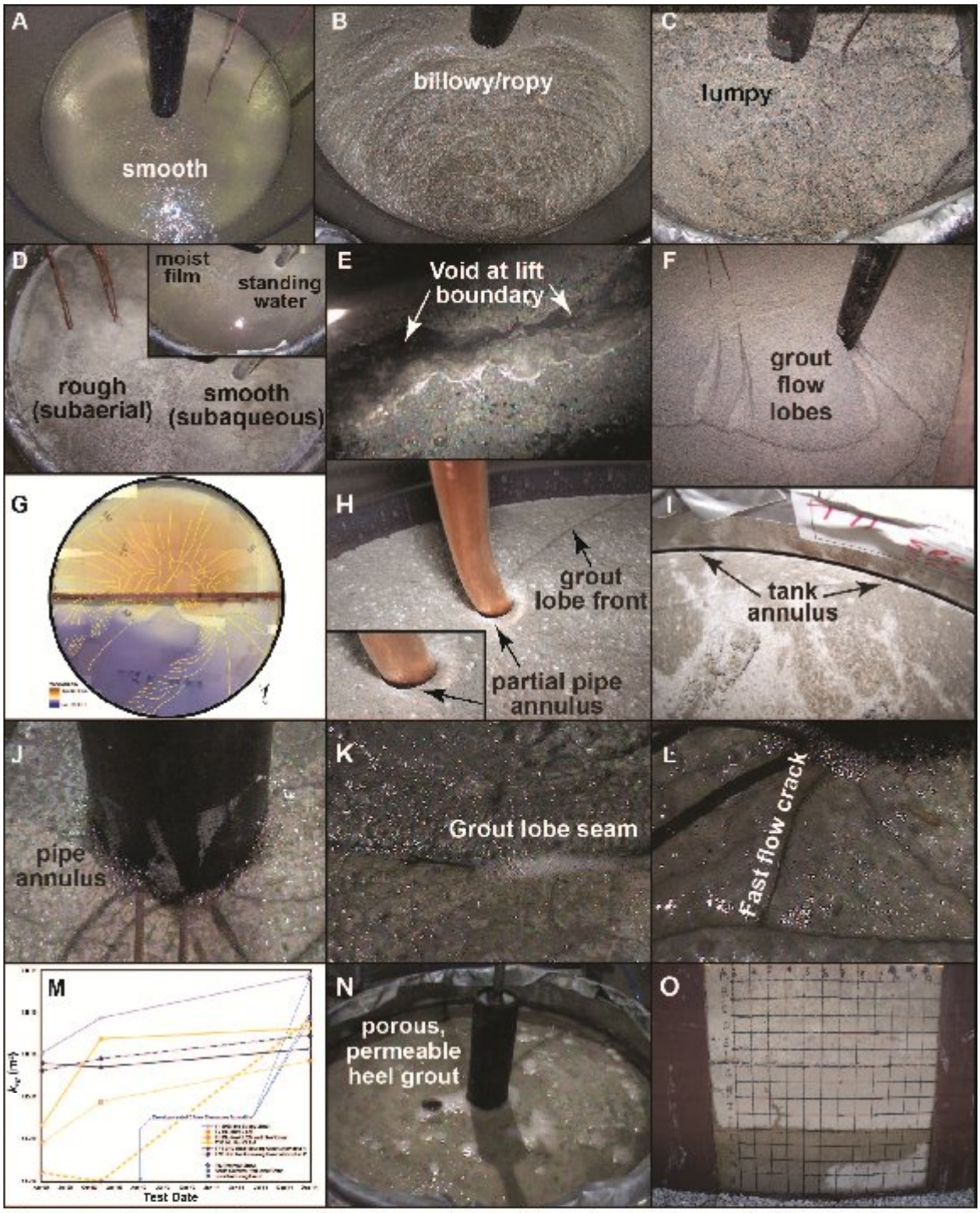

Fig. 2. Results. **(A–D)** Grout surface characteristics. **(E)** Fresh grout does not infill underlying topography. **(F)** Grout flows in lobes that split at obstacles. **(G)** Cylindrical specimen exhibits surface topography. Shrinkage results in annuli **(H)** surrounding pipes and **(I)** at the tank wall. **(J)** Internal fixtures, **(K)** grout lobe seams, and **(L)** cracks preferentially conduct fluid flow. **(M)** Bulk grout permeability increased with time post-placement. **(N)** Permeable grouts audibly conduct fluid flow. **(O)** Lift interfaces preferentially conduct fluid flow due to shrinkage, and fluids wick into cracks.

Temperature evolution was secondarily a function of conductive heat transfer between warm, newly hydrating grout lifts and cooler, newly placed grout lifts above, or cooler, older grout lifts below, suggesting the importance of grout placement schedule. Thermal modeling that accounts for the impact of grout placement schedule on peak temperature is desirable to support performance assessments of cementitious grout because temperatures generated from the heat of hydration create stresses that may lead to grout cracking if temperature gradients are too large.

Maximum temperatures and gradients attained within a hydrating grout mass and resulting thermal stresses and strains are scale dependent because the density, specific heat, thermal conductivity, and heat of hydration of the grout are dependent on the relative proportions of grout components and their properties. As a result, these parameters cannot be scaled in proportion to the dimensions of the grout specimen while also adhering to a specific grout formulation. Thus, even using insulation, the thermal processes that occur within an NDAA tank cannot be duplicated within smaller scale grout specimens unless artificially heated beyond that supplied by the heat of hydration of the small grout mass. The thermal conditions that will develop in NDAA tanks and related stresses, strains, and shrinkage cannot be duplicated in or inferred by data from bench and small- to intermediate-scale grout monolith specimens using an identical grout material in the absence of active artificial heating.

Grout Density Variations

Observations of the perimeter of the relatively large cylindrical specimen suggested that grout within lower lifts may be denser than grout within the uppermost lift; this is attributed to the role played by overburden pressure, which tends to compress air bubbles. In the absence of cracking, high-density grout may correspond to favorable porosities and permeabilities, as well as potentially smaller debonding gaps between grout and other materials.

Grout Shrinkage and Bonding

The remaining waste in NDAA tanks is on tank surfaces. At SRS, it is important for tank-stabilizing grout to bond to the steel tank liner to prevent water from entering a gap where it could rapidly flow down into the residual contamination zone at the base of the tank, bypassing conditioning that otherwise would be imparted by slow plug flow through a low-permeability reducing grout. Data suggest that because of shrinkage effects, poor bonding can occur between grout and steel tank liners and internal fixtures, as well as between grout lift and lobe seams. Some specimens developed macroscopic annuli around pipes, thermocouple wires, and drum walls. For example, 23 hrs. after an SRS-like reducing grout was placed within a drum, the grout had visibly pulled away from an embedded copper coil (Fig. 2H). Likewise, both SRS-like next-generation reducing grouts pulled away from drum walls during hydration (Fig. 2I). Ultrasonic testing revealed air gaps were present between the largest grout monolith and its steel tank liner at 53% of tested locations on a regular grid [12]. The presence of air gaps between grout and the steel tank liner is strongly suggestive of locally debonded conditions; however, the lack of an ultrasonically detected gap does not conclusively prove that a bond exists.

As grout was placed into the relatively large cylindrical tank, it spattered onto the liner and internal fixtures located above the grout surface; during subsequent placements, grout spatter eventually was surrounded by

bulk grout. Removal of the tank liner illustrated that the bulk grout mass did not always adhere well to early hydrated grout spatter, producing a vertical discontinuity and preferential flow path similar to those at grout lift and lobe seams. Grout spatter on internal fixtures also promotes formation of excess pore space because grout tends not to flow into all available void space surrounding early hydrated grout spatter. Spatter could be reduced if grout were injected only beneath the existing fresh grout surface in the discharge zone. This practice was not consistently implemented during recent grouting operations at SRS Tank 18-F, in which internal fixtures stood close to the discharge line near the tank center.

Plastic and drying shrinkage can cause annular conduits to develop inside steel tank liners and around pipes and supports. Annular gaps formed between grout and embedded pipes with apertures ranging from <1 to >50 μm. Shrinkage decreases with aggregate content and increases with the water-to-cement material (w/c) ratio. The amount and effect of plastic and drying shrinkage on the development of annular gaps is not solely a property of the material constituents, but is also influenced by the dimension and shape boundary conditions of the grout mass [15]. Larger apertures occurring in larger grout specimens are attributed to their greater volume and more potential for drying shrinkage. Differential thermal contraction of metal and grout may occur during the cooling phase, in particular, which can exacerbate poor bonding of grout to metallic components [16].

Grout Cracking

Visual inspection of the exposed surfaces of the drum and sector grout specimens did not reveal the presence of macrocracks at an early stage [4], but over a period of several years, visible cracks developed on surfaces of specimens [10] and had a significant influence on the evolution of bulk grout permeability.

In contrast, the uninsulated, outdoor cylindrical specimen developed cracks rapidly, overnight, prior to placement of subsequent lifts [8]. In the first lift, a narrow, linear crack developed overnight, prior to development of significant temperature gradients, and extended across the tank. This crack is thought to be a plastic differential settlement crack that developed above 2 of 4 plugged drains on the floor of the tank; this crack may be genetically related to two *en echelon* cracks with well-correlated positions that later developed on the surface of the third lift (Figs. 1D, 2G). On the surface of the second lift, numerous cracks formed overnight. Crack apertures were as large as 1.75 mm [8]. The surface of the third lift was cracked with shallow, wide-aperture cracks at the time the tank was uncovered 1 mo. after final grout placement. These cracks generally terminate at the base of the final grout batch without penetrating the entire third lift. Surface-intersecting cracks characterized in 2011 numbered 218 and were distributed in distinct sets (Fig. 2G), including (i) wide aperture, shallow cracks formed roughly perpendicular to lobe flow fronts, which are sometimes also radial to the monolith, (ii) the aforementioned narrow, through-going *en echelon* cracks that bisect the monolith above two plugged drains, and (iii) a few late-developed crack or fault systems semi-concentric to the monolith edge on its topographically high side [10]. Cracks oriented roughly perpendicular to lobe flow fronts and orthogonal to ropy surface ripples within the grout flow lobe commonly terminate between 0 and 10 cm behind the front of the lobe, but occasionally penetrate though the front into underlying grout. These cracks are roughly perpendicular to the tank liner as they approach it, similar to the radial cracks. The late-developed semi-concentric surface crack or fault systems paired with a very long sidewall crack or fault on the high side of the monolith may have resulted from a larger load

having been applied here [10]; these cracks or faults may have accommodated movement of a significant fraction of the grout mass from the high to low side of the monolith. Such movement would be consistent with large hydraulic conductivity estimates obtained during slug testing for two fault-intersecting coreholes.

Surface-intersecting cracks occurred more frequently in areas of relatively high topography, and frequency computed for 12 equal areas was in the range of 1–26 m^{-2}. Apertures of surface-intersecting cracks varied from <0.5–8.0 mm. Aperture values of at least 4 mm were found in each quadrant. Additional cracks are present on the surface of the cylindrical monolith now [10] relative to when it was first characterized [14]. Horizontal crack intensity estimated from vertical cores was in the range of 4–7 m^{-1} [10]; vertical/subvertical cracks were undersampled by vertical core and are best understood from the analysis of cracks that intersect the monolith surface.

Based on surface and core data from the cylindrical specimen, shallow, wide-aperture, subvertical cracks formed at the surface of every lift. Given how rapidly these cracks formed, they likely resulted from plastic shrinkage, and possibly later expanded and lengthened as a result of thermomechanical stresses and drying shrinkage once peak temperature gradients occurred and the grout had hardened. The w/c ratio of grout batches used to develop this specimen were relatively low; nevertheless any bleedwater produced at the highest elevations would have tended to flow to lower levels, leaving mounded grout relatively high and dry, and thereby more susceptible to plastic shrinkage cracking. Cracks attributed to this mechanism are of limited depth, but create connections (i.e., permeable crack networks) with grout lift and lobe seams and larger cracks caused by other phenomena. Grouting operation videos from SRS Tanks 18-F and 19-F illustrate how grout similarly mounded up locally beneath the tremie pipe. Significant bleedwater was observed to flow preferentially to the perimeters of both tanks. Relatively dry grout remaining in the high-topography center of NDAA tanks may be more susceptible to plastic and drying shrinkage cracking.

Fluid Flow and Flow Paths

Initially, gas appeared to generally flow through annular gaps (Fig. 2J) between grout and gas injection pipes. The preliminary values for annulus aperture surrounding gas injection pipes in the drum-scale specimens were in the range 1–18 μm, with INL-like CLSM exhibiting the smallest apparent apertures, and SRS-like strong grout exhibiting the largest. Annular gap solution assumptions were violated by INL-like heel grout, which was both porous and permeable. When retested after prolonged hydration, apparent annulus apertures had increased to the range 8–31 μm [10]. The calculated annulus apertures in the larger sector-shaped specimen were 14–20 μm, consistent with visual observations of these macroscopic annuli [4]. Calculated annulus apertures surrounding pipes embedded in the 12× larger cylindrical grout monolith were 20 to >50 μm, consistent with visual observation of continuously emitted particulate matter during initial pressure testing of the largest annulus [8].

The smallest containers of pressure-tested grout were 5-cm-diameter pipes filled with pipe grout; the smallest annulus apertures formed inside these (0–4.5 μm initially, increasing to 3.6–8.8 μm 6 mos. later); the smallest internal pipe apertures occurred in small drum-scale specimens while the largest occurred within pipes embedded in the larger sector specimen [8]. Likewise, external annulus apertures that formed around these pipes generally increased as the size of the container increased. Grout formulation also played

a significant role in determining the size of annuli that developed. Shrinkage-reducing admixtures [16, 17] may be utilized in next-generation grout formulations to minimize the size of annuli that develop, but DOE has postponed related efforts.

Fast flow paths in the form of cracks and permeable grout flow lobe seams were not observed on the surface of drum-scale specimens during initial testing [4]. Delayed cracking and drying shrinkage within some specimens later resulted in gas flow through cracks and grout lobe seams (Fig. 2K, L) [10]. Initially, effective gas permeabilities, k_{eg}, of drum-scale specimens were in the range 10^{-19}–10^{-16} m^2, encompassing the range reported by [5] for various strong and reducing grouts; k_{eg} values have since increased (Fig. 2M) to the range 10^{-16}–10^{-14} m^2 [10]. The INL-like CLSM specimens had the lowest values, whereas the INL-like heel and SRS-like strong grout specimens had the highest [10] (see also Fig. 2N).

Initial gas injection tests of coreholes within the cylindrical grout specimen indicated that k_{eg} in the absence of macrocracks was on the order of 10^{-18} m^2 [10]—similar to initial drum-scale specimen values and those reported by [5] for next-generation reducing grouts. The interface between the first and second lifts of grout was a significant flow pathway, rapidly transmitting tracer from coreholes to the perimeter of the specimen (Fig. 2O) where it was also observed to wick into cracks [10]. Permeability generally increased with time. Possible faults with k_{eg} on the order of 10^{-11} m^2 developed late through two coreholes [10] initially free from macrocracks. Preliminary analysis of slug test results indicated that k_{eg} of tested coreholes varied by 7 orders of magnitude, depending on degree of grout cracking, faulting, and shrinkage [10].

Drying shrinkage and the formation of conductive grout lobe seams and cracks result in a general increase with time in the size of annular gaps and the magnitude of bulk grout permeability [10]. Annulus aperture expansion with time and the presence of conductive grout lobe seams suggest that poor bonding will occur between grout and NDAA steel tank liners and any internal fixtures such as cooling coils, as well as at seams between grout lifts and flow lobes.

DOE used a gravel-based reducing grout formulation for closure of SRS Tanks 18-F and 19-F. CNWRA's SRS-like, next-generation, gravel-based reducing grout drum-scale specimens are similar (not identical) to DOE's new tank fill material. When a CNWRA specimen of this type was recently doused with water during gas injection testing, bubbles emerged both from the injection pipe annulus and locally at the drum wall. Additionally, the grout surface dried quickly, suggesting it is porous, and widespread gas bubbles emerged from the surface. Altogether, the available evidence from this specimen suggested that gas flow through both the pipe annulus and the gravel-based reducing grout was significant.

CONCLUSIONS

These experiments provided CNWRA and NRC staff with first-hand knowledge of the characteristics of grout formulations DOE has considered using to fill and stabilize NDAA tanks, including information about mixing characteristics, sensitivity of grout flowability and water–solid segregation to the w/c ratio, and lift interface characteristics and textures that develop as grout cures. Such characteristics may affect the development, distribution, and density of preferential flow pathways through NDAA grout monoliths. Staff observed grout flow lobes form, split around obstacles and reconnect at shrinkage-prone seams; fast and slow crack formation; overburden-dependent vertical density variations; air bubbles; and void space that

developed when the topography of lower lifts or lobes or grout spatter was not filled in during later grout placements. Such features yield interconnected preferential flow pathways as grout ages. Excess water in fresh grout can cause bleeding, which in turn can produce zones of increased porosity and permeability where water collects. While excess bleed water standing on the grout surface during early curing may mitigate development of plastic shrinkage cracks, it also may increase the total volumetric shrinkage that occurs during hydration and drying, leading to formation of significant annular gaps.

These experiments revealed that monolith scale is important to the macroscale heterogeneous properties of grout monoliths. The maximum temperatures attained during hydration and the fast flow pathways (i.e., cracks and annular gaps) that develop are proportional to the scale of the specimen. Annular apertures and bulk grout permeability were observed to increase with time post-placement as a function of monolith scale and grout composition. The facies architecture of grout is both a function of the scale of the monolith and the delivery mechanism—filling a 55-gal drum slowly via a narrow tremie pipe rather than quickly via a series of 5-gal buckets may have a significant effect on the scale of heterogeneities that develop. Likewise, macroscale features such as cracks and annular gaps may not be observed in bench scale specimens.

REFERENCES

1. NRC. *Technical Evaluation Report for F-Area Tank Farm Facility, Savannah River Site, South Carolina.* ML112371715. Washington, DC: U.S. Nuclear Regulatory Commission. 2011.
2. DOE Idaho. *Basis for Section 3116 Determination for the Idaho Nuclear Technology and Engineering Center Tank Farm Facility.* DOE/NE-ID-11226. Rev. 0. Idaho Falls, Idaho: DOE Idaho. 2006.
3. DOE SRS. *Basis for Section 3116 Determination for Closure of F-Tank Farm at the Savannah River Site.* DOE/SRS-WD-2012-001. Rev. 0. Aiken, South Carolina: DOE SRS. 2012.
4. Walter, G. R., C. L. Dinwiddie, E. J. Beverly, D. Bannon, D. Waiting, and G. Bird. *"Mesoscale Grout Monolith Experiments: Results and Recommendations."* San Antonio, Texas: CNWRA. July 2009.
5. Langton, C. A., A. Ganguly, C. A. Bookhammer, M. Koval, and W. L. Mhyre. *"Grout Formulations and Properties for Tank Farm Closure (U)."* WSRC–STI–2007–00641. Rev. 0. Aiken, South Carolina: Washington Savannah River Company. 2007.
6. Langton, C. A. and J. R. Cook. *"Recent Progress in DOE Waste Tank Closure."* Waste Management Symposia 2008, February 24–28, 2008, Phoenix, Arizona. WSRC–STI–2007–00686. Aiken, South Carolina: Washington Savannah River Company. 2008.
7. CH2M WG Idaho, LLC. *"Construction Specification Project No. 15722 INTEC Grout and CLSM Supply Project."* SPC–763. Idaho Falls, Idaho: CH2M WG Idaho, LLC. 2007.
8. Walter, G. R., C. L. Dinwiddie, D. Bannon, J. Frels, and G. Bird. *"Intermediate Scale Grout Monolith and Additional Mesoscale Grout Monolith Experiments: Results and Recommendations—Status Report."* San Antonio, Texas: CNWRA. September 2010.
9. Bechtel BWXT Idaho, LLC. *"Engineering Design File INTEC Tank Farm Closure Grout Mix Design."* EDF–1464. Idaho Falls, Idaho: INEEL. 2000.
10. Dinwiddie, C. L., D. R. Bannon, M. K. Todt, G. R. Walter, and M. M. Roberts. *"Fiscal Year 2012 Meso-and Intermediate-Scale Grout Monolith Test Bed Experiments: Result and Recommendations."* San Antonio, Texas: CNWRA. August 2012.
11. Bird, R. B., W. E. Stewart, and E. N. Lightfoot. "Ch. 2. Velocity Distributions in Laminar Flow." *Transport Phenomena.* New York, New York: John Wiley & Sons. 1960.

12. Dinwiddie, C. L., G. R. Walter, G. Light, W. Winterberg, D. Wyrick, D. Sims, and K. Smart. *"Bonding and Cracking Behavior and Related Properties of Cementitious Grout in an Intermediate-Scale Grout Monolith."* San Antonio, Texas: CNWRA. September 2011.
13. Walter, G. R. *"BioGas Emissions Model (BIGEM) Version 1.00 Software Validation Test Plan and Report."* San Antonio, Texas: CNWRA. 2005.
14. Dominico, P. A. and F. W. Schwartz. Physical and Chemical Hydrogeology. New York City, New York: John Wiley & Sons. 1990.
15. Neville, A. M. *Properties of Concrete.* 4th Edition. London, England: Prentice Hall. 1996.
16. Sant, G., F. Rajabipour, P. Lura, and W. J. Weiss. "Examining Time Zero and Early-Age Expansions in Pastes Containing Shrinkage Reducing Admixtures (SRAs)." *Proceedings of the 2nd RILEM Symposium on Advances in Concrete Through Science and Engineering, RILEM,* Quebec City, Canada. 2006.
17. Stefanko, D. B. and C. A. Langton. "Tank 18-F and 19-F Structural Flowable Grout Fill Material Evaluation and Recommendations." SRNL–STI–2011–00551. Rev. 0. Aiken, South Carolina: Savannah River National Laboratory. 2011.

ACKNOWLEDGEMENTS

This paper describes work performed by the CNWRA and its contractors for the NRC under Contract NRC-02-07-006. The activities reported here were performed on behalf of the NRC Office of Federal and State Materials and Environmental Management Programs. This paper is an independent product of the CNWRA and does not necessarily reflect the view or regulatory position of the NRC. The NRC staff views expressed herein are preliminary and do not constitute a final judgment or determination of the matters addressed or of the acceptability of any action that may be under consideration at the NRC. The authors acknowledge other CNWRA and SwRI staff and temporary employees who directly contributed to this research, including D. R. Bannon, D. Y. Wyrick, D. W. Sims, M. M. Roberts, D. J. Waiting, K. J. Smart, D. M. Hooper, M. R. Juckett, A. L. Hester, C. A. Burns, A. J. Galloway, G. M. Light, S. E. Winterberg, M. Morris, G. Bird, L. Gergen, M. K. Todt, E. J. Beverly, and J. Frels. The authors thank Boral Material Technologies, Inc. for fly ash; CP Kelco for Kelco-crete®; Coeur Products for core boxes; and Edwards Aquifer Authority for fluorescent dyes—all provided at no cost.

DISCLAIMER

Grout specimens were constructed using grout formulations similar to those considered for use at SRS and INL; due to differences in source materials used to mix the grouts, scale, placement rates, and environmental conditions during placement and hydration, these findings may not fully represent the behavior and properties of grouts used in the closure of NDAA tanks.